

Tsunami prediction method for earthquakes with characterized source faults (Tsunami Recipe)

English version
Translated in January, 2022.

Earthquake Research Committee, The Headquarters for Earthquake Research Promotion

This document is a translation from Japanese to English of “*波源断層を特性化した津波予測手法 (津波レシピ)*” (地震調査研究推進本部 地震調査委員会) published in January, 2017.

Tsunami prediction method for earthquakes with characterized source faults (Tsunami Recipe)

Table of Contents

Introduction.....	1
1. Configuration of characterized earthquake fault model.....	4
1.1 Macroscopic source fault characteristics	4
(a) Position and shape of the source fault model	4
(b) Size of the source fault model	5
(c) Rake Angle.....	6
(d) Average slip amount	6
(e) Rupture processes.....	8
1.2 Microscopic source fault characteristics.....	8
(a) Location and number of a large slip zone	9
(b) Slip amount and area of a large slip zone.....	10
(c) Location and number of a super large slip zone.....	12
(d) Slip amount and area of the super large slip zone.....	13
2. Tsunami simulation and uncertainties in the tsunami prediction.....	15
2.1 Tsunami simulations	15
(a) Computational area and grid spacing	15
(b) Discretization of topographic and bathymetric data.....	15
(c) Crustal movement and distribution of initial water height.....	16
(d) Baseline tidal level	16
(e) Simulations for tsunami propagation and run-up	16
(f) Boundary conditions	18
(g) Coefficient of roughness	18
(h) Length of computation time and computational time step interval.....	19
2.2 Uncertainties in tsunami predictions	20
3. Validation of the characterized earthquake fault model	21
4. Appendix: Validation of the tsunami prediction method for earthquakes with characterized source faults (Tsunami Recipe).....	22
5. References	25

Introduction

In the past, many large earthquakes have occurred in marine areas around Japan, including the 2011 off the Pacific coast of Tohoku Earthquake, and the accompanying tsunamis have caused serious damage.

Figures 1 and 2 show recorded trace heights from past major tsunamis plotted onto the map of Japan. Past impacts in the region can be observed from these figures. However, there are limits to historical documentation, and some past tsunami records may be either unclear, or the tsunamis may not be recorded in the first place. Therefore, predictions of future tsunami possibility, created using records from the past, may be affected. A concept and approach that compensate for this limitation, and that take the associated uncertainty into account, are needed.

Note that trace heights shown in Figures 1 and 2 include the tsunami height, trace height, and run-up height, as defined in Figure 3.

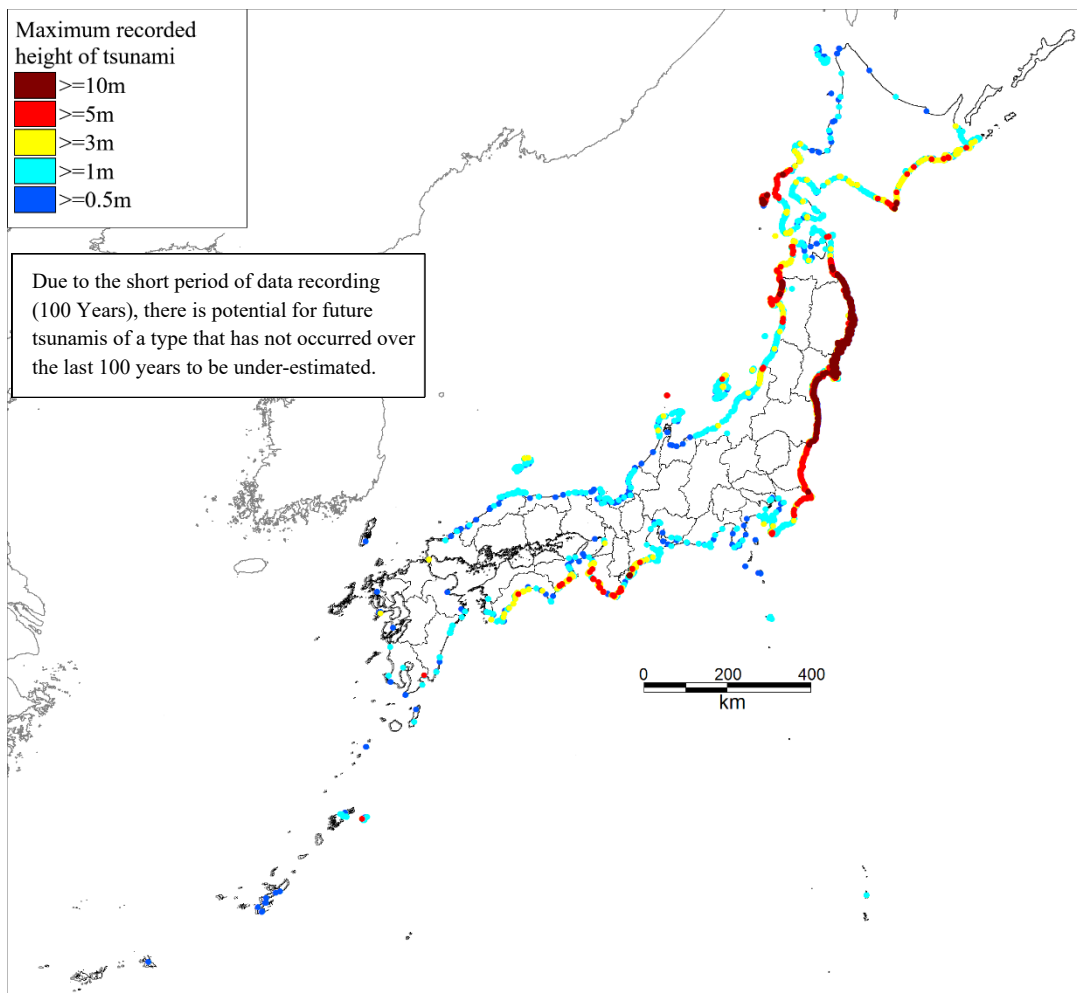


Figure 1. Trace heights and location records for tsunamis over 50 cm that have occurred since 1896

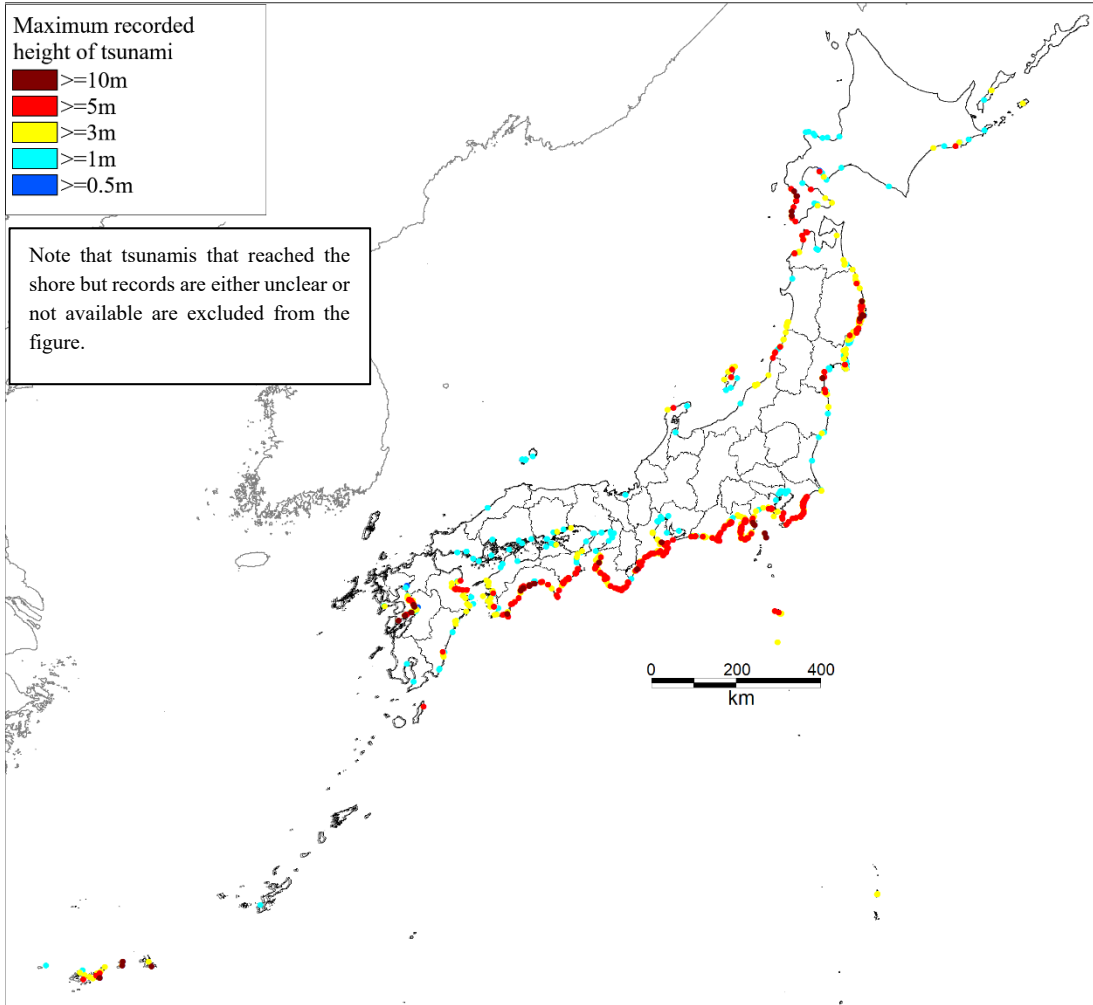


Figure 2. Trace height and location records for tsunamis over 50 cm that occurred in or before 1895

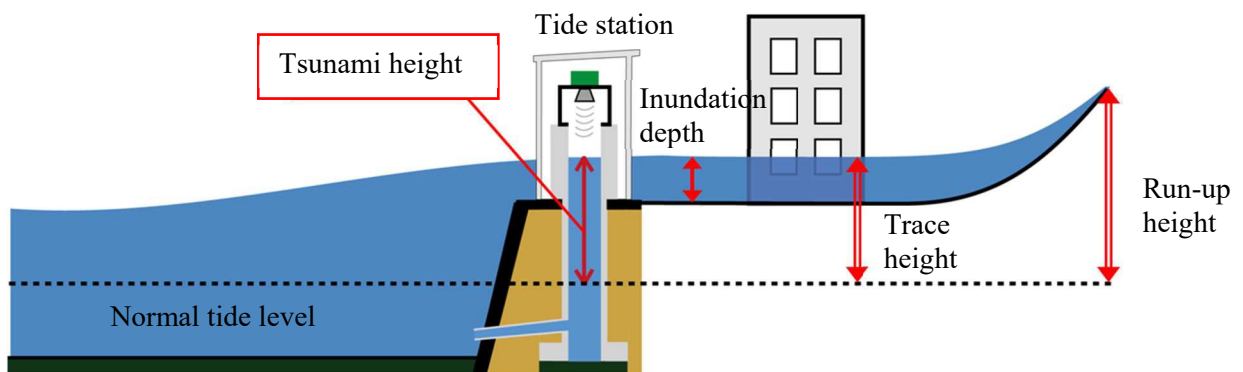


Figure 3. Relationship between the tsunami height at a tidal station, the inundation depth, the trace height, and the run-up height (from the Japan Meteorological Agency website)

The Earthquake Research Committee (ERC) has compiled a long-term evaluation of potential future earthquake occurrences (i.e. long-term evaluation), and the committee has plans to also evaluate associated tsunami risks, based on this long-term evaluation. In general, for a future earthquake, the slip distribution of a fault cannot be determined with certainty, and this is why this study "Tsunami prediction method for earthquakes with characterized source faults (tsunami recipe)" has been prepared. In doing so, the authors have considered methods for the prediction and evaluation of tsunamis which have been based on many earthquake fault models using simplified parameters, while also accounting for uncertainty.

Tsunami recipe is a method for prediction and evaluation which can be applied by the ERC to evaluate the risk of the various tsunami types which accompany earthquakes. The method includes both the largest class of tsunami, and tsunamis of low height and high frequency, which also cause damage; it includes descriptions of how and when the method is to be utilized and the concepts under which it was derived. A "prediction" refers to a calculated expectation of tsunami height at the coast after an assumed earthquake, while an "evaluation" refers to an estimate which has taken various uncertainties, such as the computational errors included in tsunami predictions, into account. While the method is applied mainly to interplate earthquakes for now, it will be revised in the future to expand the types of earthquakes covered. Given that the knowledge available for potential future faults and earthquakes, and associated tsunamis, is insufficient, it would be ideal to configure a default source of prediction variables, by considering and determining the computational approach and potential results now, for cases where variations in the phenomena and associated uncertainties need to be considered.

In recent years, various institutions have proposed configurations for fault models and computational methods – for the largest class of tsunamis in particular (e.g. Cabinet Office, 2012; Ministry of Land, Infrastructure, Transport and Tourism, 2012).

Figure 4 shows the process used for tsunami prediction and evaluation in the tsunami recipe, as a flowchart, while the following section explains the steps of the chart.

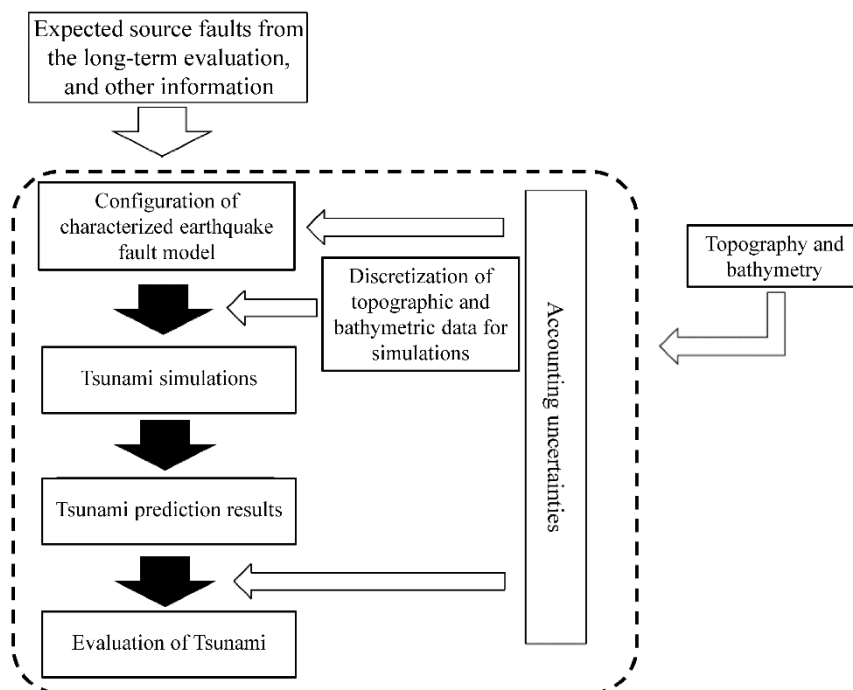


Figure 4. Flowchart for tsunami prediction and evaluation using the tsunami recipe

1. Configuration of characterized earthquake fault model

A "characterized earthquake fault model" is a source fault model that represents the characteristics of source faults through major parameters. In the tsunami recipe, "source fault" refers to the fault of an earthquake that causes a tsunami. Model parameters are configured by considering macroscopic source fault characteristics that represent the location, shape, and size of the source fault overall, as well as microscopic source fault characteristics that mainly represent the unevenness of the slip distribution of the source fault. In a tsunami recipe, a characterized earthquake fault model is expressed by combining one or more rectangular element faults, whose sides are parallel to the sea floor.

The approach to configuration of source fault characteristic parameters, as explained here, is shown specifically to construct a characterized earthquake fault model for a tsunami that occurs due to an assumed earthquake. For consideration of a characterized earthquake fault model, the concept of "Strong ground motion prediction method for earthquakes with specified source faults ("Recipe")" (Earthquake Research Committee, 2016), was utilized as a reference.

In particular, as represented by many interplate earthquakes, information on past earthquakes are available, depending on the marine area. This information can be utilized in configuring the characteristic earthquake fault model. As explained in Section 3, the model is validated, as needed, by using data related to past tsunamis, and source fault characteristic parameters are revised if needed. In such a situation where a characteristic earthquake fault model is revised, an investigation may sometimes take place by going beyond the tsunami recipe, as source fault characteristic parameters that can explain observational data for a tsunami are required. In this case, some of the relevant data from past tsunamis (such as the size of the earthquake, the source area of the tsunami, the tsunami record, trace height, damage, etc.) may not be consistent with other data, and data needs to be utilized by assigning priorities, depending on the objective, such as prediction or evaluation.

A similar consideration is also underway in the field of nuclear safety assessment, where a characterized wave source model, that takes broad tsunami characteristics into account, is being investigated (e.g. Sugino et al., 2014; Japan Society of Civil Engineers, 2016)

1.1 Macroscopic source fault characteristics

The following parameters are configured as the macroscopic source fault characteristics for the source fault model:

- Position and shape of the source fault model (length, width, strike and dip angles)
- Size of the source fault model (fault area, seismic moment)
- Rake angle
- Average slip amount
- Rupture process

(a) Position and shape of the source fault model

Position, length, width, strike, and dip angles of a source fault model are configured based on the fault parameters for an assumed earthquake, if the parameters are estimated. For an interplate earthquake, the source fault model is configured to correspond to the upper surface of the oceanic plate, estimated by seismic surveys and hypocenter distribution.

If the evaluation result for position and shape of the source area is shown by a long-term evaluation, the result should be noted.

(b) Size of the source fault model

The size of the source fault model (fault area, seismic moment) is configured by one of the following methods.

Method 1: Clearly define the range of the source fault by position and shape in the source fault model, calculate the area equivalent to that range, and estimate the seismic moment using the empirical relationship between the seismic moment and the fault area.

Method 2: For an earthquake in which determining the seismic source fault is difficult, configure the seismic moment, and configure the area of the tsunami source fault by using an empirical relationship between the seismic moment and the fault area.

To establish the empirical relationship between the seismic moment M_0 (N · m), and fault area S (m²), use an equation that considers the local characteristics, if some level of past earthquake data is available. For example, a local relationship between seismic moment M_0 (N · m) and fault area S (m²) may be configured by estimating an average stress drop $\Delta\sigma$ (MPa) for an earthquake that occurs in the area coverage based on equation (1) (Eshelby, 1957), which assumes a circular failure surface, similar to Kanamori and Anderson (1975).

$$M_0 = 16/(7\pi^{3/2}) \cdot \Delta\sigma \cdot S^{3/2} \quad (1)$$

On the other hand, if little or no past earthquake data is available, an empirical relationship for a seismic moment M_0 (N · m) that shows an average characteristic, and fault area S (m²), is used (e.g. Sato, 1989; Yamanaka and Shimazaki, 1990; Murotani et al., 2008, 2013).

However, caution needs to be exercised in selecting the range of values for seismic moment and fault area within the data set from which the empirical relationship was developed.

For example, working in a manner similar to Yamanaka and Shimazaki (1990), configuring an empirical relationship such that equation (1) holds by using seismic moment M_0 (N · m) and fault area S (m²), as organized by Sato (1989) for interplate earthquakes that occurred on the Pacific side around Japan and adding more data to it, yields a result of $M_0 = 1.77 \times 10^6 \cdot S^{3/2}$ ($\Delta\sigma = 4.3$ MPa) (Fujiwara et al., 2015). The value is set at $\Delta\sigma = 3.0$ MPa by the Committee for Modeling a Nankai Trough Megaquake (second report) (Cabinet Office, 2012), and these values can be referenced.

However, the empirical relationship between seismic moment and fault area represents an average relationship established with data from several past earthquakes, and individual earthquakes may vary around this relationship. For this reason, caution needs to be exercised over the fact that prediction results contain a similar variance when predicting future tsunamis using an empirical relationship, and that the empirical relationship itself is still at the research stage.

Empirical relationships in which the seismic moment is proportional to a power of 3/2 of a fault area, as shown in the equation, correspond to the fact that the ratio of length and width of a fault, and the average stress drop at the source fault, is constant, regardless of the size of the earthquake. However, the width of a fault is restricted by the depth of the upper and lower ends, and the ratio of length and width may not be constant in a giant-size earthquake so that the empirical relationship between seismic moment and fault area may be different. In fact, the empirical relationship between seismic moment and fault area in relatively large inland crustal earthquakes (over magnitude M_w 6.5) is known to differ from the relationship for smaller size earthquakes (e.g. Irikura and Miyake, 2001; Tajima et al., 2013). Observational data is limited for giant-size

interplate earthquakes in which the width of a fault reaches an upper limit. Some studies have suggested that seismic moment can be explained, within the range of variance, by the relationship where a seismic moment is proportional to the power of 3/2 of a fault area, for cases including giant earthquakes that have occurred globally since 1950 (Murotani et al., 2013). Other studies have proposed a relationship in which a seismic moment is the square of the fault area, for earthquakes of a certain size (Tajima et al., 2013), ultimately leading to multiple interpretations of the relationship. On this basis, referencing multiple concepts is a preferred approach for configuring a source fault model for great and giant earthquakes.

Some studies have pointed out that the relationship between observed seismic moment and fault area is different between an interplate earthquake and an intraplate earthquake (e.g. Iwata and Asano, 2011). They have suggested that caution should be exercised over what earthquake was used for the base data set, when using an equation that takes locality into account, by utilizing past earthquake data from the location. Estimated values for observed seismic moment and fault area should also be treated carefully, by recognizing that the values vary depending on the data used for analysis, such as ground motion, tsunami, and geodetic data.

The relationship between moment magnitude M_w , and seismic moment M_0 (N·m), is expressed by the following equation.

$$\log M_0 = 1.5 \cdot M_w + 9.1$$

(c) Rake Angle

In the case of an interplate earthquake, estimate rake angle from a momentum vector relative to the plate motion, and the shape of the plate boundary. If the values are presented for a long-term evaluation, note them accordingly.

If the data on the rake angle are not available, the type of fault in the interplate earthquake is treated as a reverse fault, and the rake angle is assumed to be 90° (Earthquake Research Committee, 2016).

The rake angle in a source fault of an actual earthquake varies depending on the location on the fault plane.

(d) Average slip amount

The relationship between the average slip amount, D (m), and seismic moment, M_0 (N·m), for the entire source fault can be expressed using the area of the source fault, S (m²), and modulus of rigidity μ (N/m²):

$$D = M_0 / (\mu \cdot S) \tag{2}$$

The modulus of rigidity is assumed to be a standard value for the medium in the area where a source fault is distributed, and is calculated by the following equation, using the density, ρ (kg/m³), of the earthquake occurring layer, and S wave velocity β (m/s):

$$\mu = \rho \cdot \beta^2 \tag{3}$$

Standard values for the modulus of rigidity of the medium in the marine areas around Japan can be referred to – such as from a resource by the Japan Society of Civil Engineers (2016). The modulus of rigidity of the medium around the plate boundary surrounding Japan, based on the Japan integrated velocity structure model (provisional version) (Earthquake Research Committee, 2012), is shown in Table 1.

Table 1. Modulus of rigidity of the medium around plate boundaries surrounding Japan

Depth (references classification by the Japan Society of Civil Engineers, 2016)	Physical values by the Japan integrated velocity structure model (interim version)	Modulus of rigidity
Depth of the entire fault plane is less than 20 km	Physical value of the upper crust $\beta = 3.4 \text{ km/s}$ $\rho = 2.7 \text{ g/cm}^3$ $\rightarrow \mu = 3.12 \times 10^{10} \text{ N/m}^2$ Physical value of the lower crust $\beta = 3.8 \text{ km/s}$ $\rho = 2.8 \text{ g/cm}^3$ $\rightarrow \mu = 4.04 \times 10^{10} \text{ N/m}^2$ Values will be an intermediate of the above.	$3.5 \times 10^{10} \text{ N/m}^2$
Depth of the entire fault plane is deeper than 20 km	Physical value of the mantle $\beta = 4.5 \text{ km/s}$ $\rho = 3.2 \text{ g/cm}^3$ $\rightarrow \mu = 6.48 \times 10^{10} \text{ N/m}^2$	$6.5 \times 10^{10} \text{ N/m}^2$
Entire fault plane is spread over above and below the 20 km depth	Values will be an intermediate of the above.	$5.0 \times 10^{10} \text{ N/m}^2$

No cases have been found where the average slip of a giant earthquake significantly exceeded 10 m, although average slips for giant earthquakes are being studied currently.

A study that has estimated the modulus of rigidity near a plate boundary by an analysis of many interplate earthquakes has shown that it increased with depth (Bilek and Lay, 1999). When the shallow part of the plate boundary is included in the source fault, caution should be exercised, owing to the fact that a large slip, relative to the size of the earthquake, may occur as a result of a small modulus of rigidity. In cases where unconsolidated sediments are found near the trench axis, deformation of the sediments also contributes to a greater tsunami (for example, Fukao, 1979). An earthquake that causes a large tsunami relative to the size of the ground motion is generally called a tsunami earthquake, but its generation conditions are currently under research, as various causes have been proposed.

If tsunami magnitude, M_t , is available as an earthquake size information, in addition to the position and shape of the source fault in a tsunami earthquake, Sections 1.1 (b) and (d) can be omitted, and the average slip can be adjusted such that tsunami magnitude, M_t , calculated from the tsunami height, etc. by tsunami simulation, can match that information.

(e) Rupture processes

While there is diversity in the rupture processes of an earthquake, a characterized earthquake fault model that expresses the characteristics of a source fault by major parameters typically assumes that a slip across the entire source fault occurs simultaneously and instantaneously. However, caution should be exercised on the impact of the difference in rupture velocity on the tsunami simulation.

Rupture velocity is generally faster than the propagation velocity of a tsunami, and therefore is calculated by assuming that the slip across the entire source fault occurred simultaneously. For example, recent studies have shown that the difference in rupture velocity had little impact on the waveform of the tsunamis from either the 2003 Tokachi-oki earthquake, or the 2014 Iquique earthquake (Tsushima et al., 2012; Gusman et al., 2015). On the other hand, the impact of the difference in rupture velocity on the tsunami waveform cannot be ignored in cases where a tsunami that occurs on a large source fault, or a source fault near the coast, is calculated in detail. When taking a finite rupture velocity into account, arrival time of the tsunami is typically slower, while maximum wave height is large in the direction of propagation and small on the opposite side, compared to the case in which rupture velocity is assumed to be infinite (e.g. Kawata et al., 2006; Suppasri et al., 2011). Development of a method for calculating finite rupture velocity is a challenge for the future.

There is a directivity to energy propagation in a tsunami that accompanies an earthquake, and in general, the majority of the energy is propagated in the direction of the short axis of the source fault, while a minority of the energy propagates along the long axis (Kajiura, 1970; Ben-Menahem and Rosenman, 1972). When accounting for the impact of rupture propagation, directivity of the energy propagation in a tsunami should be noted, and its impact needs to be taken into consideration along the direction in which the larger amount of energy propagates.

In a case where a slip occurs instantaneously, rise time (the time for which slip continues at the location where the fault surface exists) becomes 0.

1.2 Microscopic source fault characteristics

Microscopic characteristic parameters for a source fault model include the following:

- Location and number of the large slip zone
- Slip amount and area of the large slip zone

A large slip zone is configured to account for the impact of heterogeneous slip distribution on the occurrence of a tsunami and is an area with large slip compared to the background. At its simplest, a two-stage slip distribution is assumed here, where the slip amount in the large slip zone and the background zone are uniform.

In one case where the fault rupture nearly reached the trench axis, a very large slip occurred near the trench axis, and caused a very large tsunami (e.g. Satake et al., 2013). In order to account for the impact of such a slip on the occurrence of a tsunami, a super large slip zone, where the slip amount is even greater, is assumed within a large slip zone defined along the trench axis. In this case, the following parameters are configured, in addition to the parameters discussed above:

- Location and number of the super large slip zone
- Slip amount and area of the super large slip zone

For the simplest case, a three-stage slip distribution is assumed here, where the slip amount in the super large slip zone, the large slip zone, and the background zone, are uniform.

Note that the Cabinet Office (2012) allocated conceptual large slip zones and super large slip zones to the largest class of tsunami, when considering government measures to be allocated against disaster prevention.

(a) Location and number of a large slip zone

In order to express the diversity of slip distribution for future earthquakes, several characterized earthquake fault models have been configured with different large slip zone positions.

A large slip zone takes a shape that aligns with the area of the characterized earthquake fault model, and a single area is defined in the model. However, for a long-term evaluation, multiple large slip zones may be configured for giant earthquakes that rupture multiple segments at once.

For example, a large slip zone is configured such that it overlaps along the strike direction of the source fault for approximately half the length of the large slip zone, while deep, middle, and shallow parts are defined in the dip direction (as shown in Figure 5; however, a total of $n \times 3$ patterns are configured, if n patterns are configured in the strike direction). An evaluation method that takes differences in probability of occurrence of each model into account should be addressed in the future.

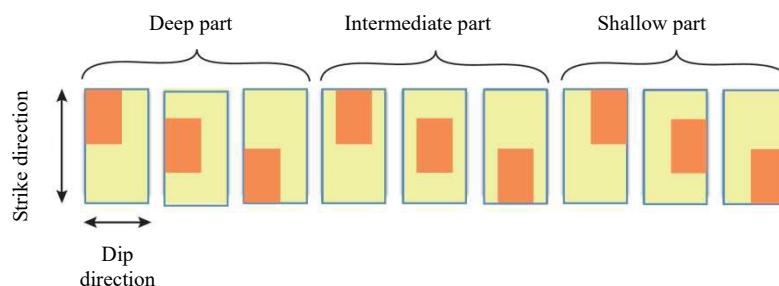


Figure 5. Examples of configured large slip zones: Orange areas are large slip zones, and yellow areas represent the background zone

In a case where the result of tsunami simulation does not change significantly by altering the location of a large slip zone for relatively small earthquakes, multiple characterized earthquake fault models, where different locations of a large slip zone are configured, can be represented by a single model, once the differences in the results of predictive calculations due to differences in the location of a large slip zone have been verified.

If the source fault is shallow, and land is located immediately above the fault, the difference in the location of the large slip zone may have a significant impact on the result of a tsunami simulation. When conducting detailed evaluation of a tsunami in such a location, conditions for configuration of the location of a large slip zone need to be investigated individually, to account for the impact of having a large slip zone in such a diverse location on the evaluation point.

Given that the coupling rate of the fault plane is higher than that of the surroundings, in an area that becomes a large slip zone when an earthquake occurs, the location in which slip deficit is large can be assumed to be the large slip zone if the distribution of slip deficit can be estimated based on crustal movement data. For example, recent studies based on the analysis of observed crustal movement data have reported that an area with a large slip deficit prior to a great earthquake became the source area for a great earthquake and slipped significantly (Hashimoto et al., 2009; Nishimura, 2012). In the case of an interplate earthquake, a gravity anomaly data may also be referenced, since a corresponding relationship has been pointed out between an area with a negative gravity anomaly and the location of a large slip zone in the source area of the interplate earthquake (e.g. Wells et al., 2003; Sugiyama, 2004; Song and Simons, 2003).

When estimating the distribution of a slip deficit off the coast from a location with terrestrial crustal movement data, a constraint condition exists whereby the slip deficit near the trench axis is set to 0 in some cases to avoid an unstable solution – and therefore, caution is advised when using such data.

(b) Slip amount and area of a large slip zone

Slip amount for a large slip zone, D_L (m), is represented as an average slip, D (m), of the entire source fault, multiplied by ζ_L , and the value of ζ_L is defined based on the area ratio per slip amount, using analysis based on observational data from past, great earthquakes.

$$D_L = \zeta_L \cdot D \quad (4)$$

Next, a large slip zone, S_L (m²), is represented as the product of the area, S (m²), for the entire source fault, multiplied by r_L , and the value of r_L is defined, based on the area ratio per slip amount, by the result of an analysis based on observational data from past great earthquakes.

$$S_L = r_L \cdot S \quad (5)$$

Area of the background zone, S_B (m²), can be calculated by the following equation:

$$S_B = S - S_L \quad (6)$$

Slip amount D_B (m) for the background is calculated by the following equation, which uses the area, S_B (m²), and seismic moment, M_{0B} (N · m), of the background, where the latter is obtained by subtracting the seismic moment M_{0L} (N · m) of the large slip zone from the seismic moment M_0 (N · m) for the entire source fault. The value of the modulus of rigidity, μ (N/m²), is obtained from equation (3) in Section 1.1 (c).

$$M_{0L} = \mu \cdot D_L \cdot S_L \quad (7)$$

$$M_{0B} = M_0 - M_{0L} \quad (8)$$

$$D_B = M_{0B} / (\mu \cdot S_B) \quad (9)$$

By substituting equations (2) and (4)–(8) into equation (9), the following equation is obtained as the relationship between the slip amount, D_B (m), in the background zone, and the average slip, D (m), for the entire source fault.

$$D_B = (1 - \zeta_L \cdot r_L) D / (1 - r_L) \quad (10)$$

Based on tsunami inversion analysis of past great earthquakes, Figure 6 shows the area ratio (cumulative area ratio) of the element fault with slip amount over a certain ratio, against the entire fault, presented in descending order of the normalized slip amount of element faults. The slip amount in a characterized earthquake fault model is expressed as a step function, and each parameter should be configured such that they approximate the result of analysis.

For example, the function in Figure 6 is generally approximated by configuring the parameters such that $\zeta_L = 2$, and $r_L = 0.3$. As a result, in this example, a large slip zone would be configured such that the slip amount was double the average slip for the entire source fault and the area was 30% of the entire source fault.

In "Strong ground motion prediction method for earthquakes with specified source faults" ("Recipe") (Earthquake Research Committee, 2016), the average slip for the entire asperity is also defined as double the average slip for the entire seismic source fault.

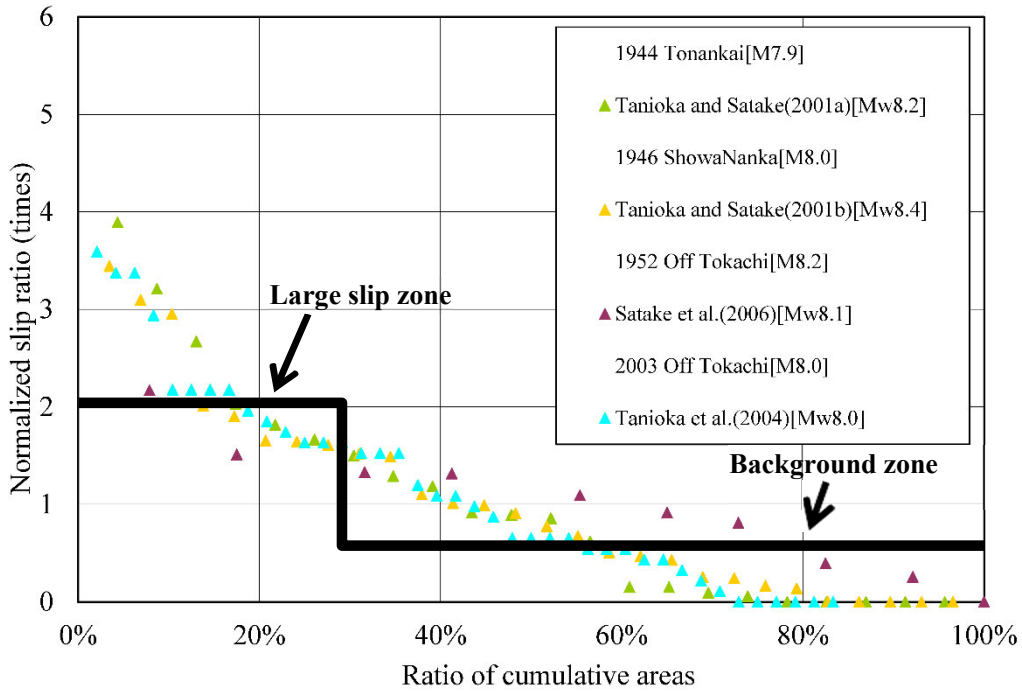


Figure 6. Distribution of normalized slip ratio and cumulative integrated ratio for great earthquakes. The bold black line in the figure represents the parameters for the characterized earthquake fault model

The size of earthquakes in the legend is shown as M, by the Japan Meteorological Agency, and M_w by analysis.

(c) Location and number of a super large slip zone

Super large slip zones are defined to consider extremely large slips near a trench axis, and a single area can be defined within a single large slip zone in a manner such that it is adjacent to the upper end of the large slip zone in a dip direction.

A super large slip zone typically features a shape that aligns with the large slip zone.

In order to account for diverse slip distributions, large slip zones and super large slip zones are configured in a manner such that a large slip zone overlaps for approximately half the length of the super large slip zone in the strike direction (as shown in Figure 7).

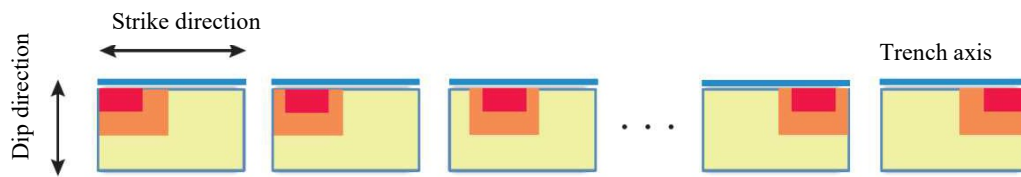


Figure 7. An example of configuration of a super large slip zone: Red represents the super large slip zone, orange represents the large slip zone, and yellow represents the background zone.

(d) Slip amount and area of the super large slip zone

Slip amount, D_S (m), in the super large slip zone is represented as an average slip, D (m), of the entire source fault, multiplied by ζ_S . The slip amount, D_L' (m), in the large slip zone is represented as an average slip, D (m), of the entire source fault, multiplied by ζ_L' , ζ_S and ζ_L' values are defined based on the area ratio by slip amount, from analysis results on observed cases of past giant earthquakes.

$$D_S = \zeta_S \cdot D \quad (11)$$

$$D_L' = \zeta_L' \cdot D \quad (12)$$

Next, the super large slip zone, S_S (m²), is represented as the product of the area of the source fault, S (m²), and r_S , and the large slip zone, S_L' (m²), is represented as the product of the area of the source fault, S (m²), and r_L' . Then r_S and r_L' values are defined, based on the area ratio by slip amount from analysis based on observed cases of past giant earthquakes.

$$S_S = r_S \cdot S \quad (13)$$

$$S_L' = r_L' \cdot S \quad (14)$$

The area of the background zone, S_B' (m²), can be calculated by the following equation:

$$S_B' = S - S_S - S_L' \quad (15)$$

Slip in the background zone, D_B' (m), is calculated by the following equation, using the area of the background zone, S_B' (m²), and the seismic moment of the background zone, M_{0B}' (N · m). The latter parameter is obtained by subtracting the seismic moment of the super large slip zone, M_{0S} (N · m), and the seismic moment of the large slip zone, M_{0L}' (N · m), from the seismic moment for the entire source fault, M_0 (N · m). The value of the modulus of rigidity μ (N/m²) is the value obtained from equation (3) in Section 1.1 (c).

$$M_{0S} = \mu \cdot D_S \cdot S_S \quad (16)$$

$$M_{0L}' = \mu \cdot D_L' \cdot S_L' \quad (17)$$

$$M_{0B}' = M_0 - M_{0S} - M_{0L}' \quad (18)$$

$$D_B' = M_{0B}' / (\mu \cdot S_B') \quad (19)$$

Equation (20) is then obtained as the relationship between the slip amounts in the background zone, D_B' (m), and the average slip, D (m), for the entire source fault, by substituting equations (2) and (11)–(18) into equation (19):

$$D_B' = (1 - \zeta_S \cdot r_S - \zeta_L' \cdot r_L') D / (1 - r_S - r_L') \quad (20)$$

Based on tsunami inversion analysis of past giant earthquakes, Figure 8 shows the area ratio (cumulative area ratio) of the element fault with a slip amount over a certain ratio, against the entire fault, presented in descending order of the normalized slip amount of element faults. The slip amount in a characterized earthquake fault model is expressed as a step function, and each parameter should be configured such that they approximate the results of analysis.

For example, the function in Figure 8 is generally approximated by configuring parameters as $\zeta_S = 4$, $r_S = 0.1$, $\zeta_L = 2$, and $r_L = 0.2$. This means that, in this example, the super large slip zone could be configured such that the slip amount was 4 times the average slip for the entire source fault, the area was 10% of the entire source fault, while the large slip zone could be configured such that the slip amount was double the average slip for the entire source fault, and the area was 20% of the entire source fault (i.e. the super large slip zone and large slip zone together account for 30% of the entire source fault).

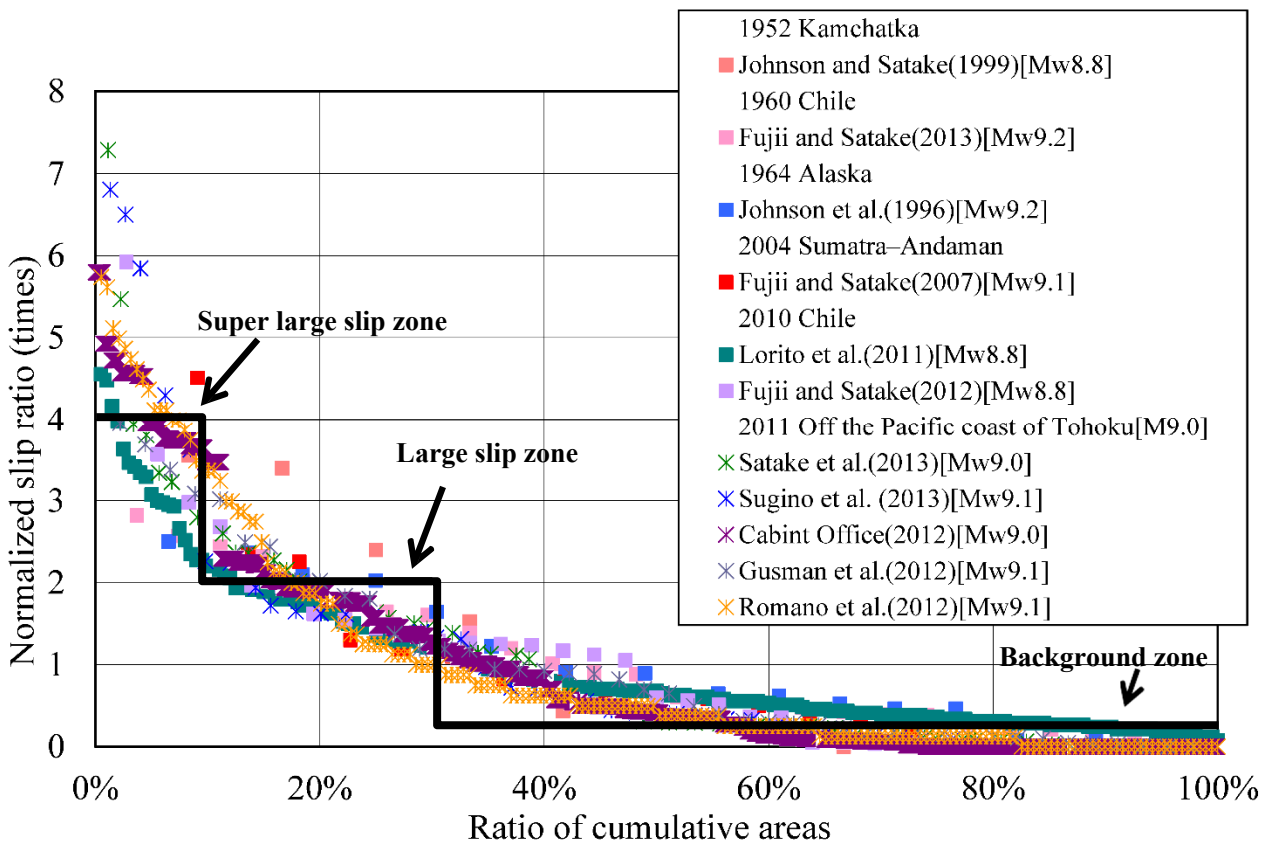


Figure 8. Distribution of normalized slip ratio and cumulative integrated ratio for giant earthquakes. The bold black line represents the parameters for the characterized earthquake fault model

The size of earthquakes in the legend is shown as M by the Japan Meteorological Agency, and M_w by the result of the analysis adopted.

2. Tsunami simulation and uncertainties in the tsunami prediction

This chapter explains the method of tsunami simulations and its uncertainties. In this method, a topography model is developed for marine and terrestrial areas first, and then crustal movements and the distribution of initial water height are calculated, based on a source fault model configured in "1. Configuration of characterized earthquake fault model". Also, the propagation and run-up of a tsunami are calculated to predict the coastal tsunami height. Results from tsunami simulations based on numerical computation include uncertainties such as computational errors, and the section explains this factor as well.

2.1 Tsunami simulations

(a) Computational area and grid spacing

Computational area and computational grid spacing in tsunami simulations are configured so that tsunami behaviors such as refraction, reflection, and run-up, etc. are calculated with good accuracy, while taking features such as the size of the wave source area and topography of the sea floor and shores into account.

The ideal computational grid spacing for tsunamis is known to be less than $1/20$ of a single wavelength of a tsunami (Hasegawa et al., 1987). Tsunami wavelengths become shorter as water becomes shallower, and nesting would be the ideal approach where areas with different computational grid spacing (that vary depending on the wavelength and topography of the tsunami) are connected and computed simultaneously. When nesting, a method in which computational grid spacing is reduced by a ratio of $1/3$ or $1/2$ is used, since short wavelength components that occurred in a small area may be trapped within the small area without propagating to a larger area.

Computational grid spacing needs to be configured appropriately for the required computational accuracy. It has been configured as 1350 m, 450 m, 150 m, and 50 m from the open ocean to coastal areas in the appendix case, since its objective was to provide an overview of tsunami height across Japan.

When calculating the run-up, computational grid spacing in a terrestrial area needs to be configured smaller by approximately 10 m (e.g. Ministry of Land, Infrastructure, Transport and Tourism, 2012). However, no significant difference has been observed, in terms of either the coastal level or the maximum water level in particular, due to differences in terrestrial computational grid spacing (Murashima et al., 2006).

(b) Discretization of topographic and bathymetric data

The topographic and bathymetric data have a significant impact on the results of calculation for the propagation and run-up of tsunamis, and are therefore discretized appropriately, based on the latest surveys and studies. The topographic data are typically produced from high-precision elevation data, obtained by airborne LiDAR survey, etc.

Generally, elevation of the terrestrial area is determined using the Tokyo Peil (T.P.) as the reference plane, and the height of the sea surface in the marine area (tidal level) is determined using the datum line (D.L.) established for each tidal station as the reference plane. Tsunami predictions need to be calculated by treating marine areas and terrestrial areas as a whole, and the topographic and bathymetric data used generally uses the T.P. as the reference plane.

Coastal structures are usually included as needed.

(c) Crustal movement and distribution of initial water height

Estimation of the distribution of initial water height generally considers the contribution in vertical direction from the horizontal crustal displacement of the seafloor slope to the vertical crustal displacement (uplifting and settling) at sea floor calculated by the source fault model.

Methods for calculating the crustal movement that appears on the surface of an elastic half-space body by the source fault model include Sato (1971), Sato and Matsu'ura (1973), Yamashita and Sato (1974), and Mansinha and Smylie (1971), while a program by Okada (1985, 1992) is used widely. Slip amount is uniform in all of these methods, where the theoretical formula addresses a rectangular fault where one side is parallel to the ground surface. For calculations of the crustal movement that corresponds to a more realistic source fault model, in which the complex shape of the plate boundary surface and the slip amount vary by location, the source fault is divided into small rectangular and triangular element faults (Thomas, 1993; Meade, 2007). These small faults are aligned to match the configuration of the upper surface of the oceanic plate as much as possible, and the results from individual calculations are combined by configuring the slip amount per element fault.

However, in places where the shape of the upper surface of the oceanic plate changes rapidly, and for boundaries where the configured slip amount changes significantly, crustal movement of the sea floor obtained by overlapping rectangular faults depends greatly on the placement of element faults. In such cases, caution needs to be exercised in that actual fault movement cannot be modeled efficiently – and so an unrealistic crustal movement may be obtained in some cases.

If the contribution of the horizontal crustal movement to the vertical displacement of the sea floor is $u_h = u_x \frac{\partial H}{\partial x} + u_y \frac{\partial H}{\partial y}$, then the initial water height is expressed as $u_z + u_h$ (Tanioka and Satake, 1996). Here, u_x and u_y are displacements of the sea floor in a horizontal direction (x-axis direction and y-axis direction, respectively), u_z is the displacement of the sea floor in vertical direction, and H is the water depth.

If the spatial movement wavelength of the crustal movement has become significantly shorter, compared to the wavelength of tsunami propagation, the hydraulic filter developed by Kajiura (1963) should be applied to the amount of crustal movement, and the result should be treated as an initial water height.

(d) Baseline tidal level

Baseline tidal level typically uses the Tokyo Peil (T.P.).

Baseline tidal level can also be set as the mean sea level (M.S.L.), at that point. Tidal conditions should be configured appropriately, depending on the use of the results from tsunami simulations.

In a tsunami simulation, the tidal level used to configure an assumed tsunami inundation should, in general, be the high water level (H.W.L.) (Ministry of Land, Infrastructure, Transport and Tourism, 2012).

(e) Simulations for tsunami propagation and run-up

Simulations for the propagation and run-up of tsunamis are based on nonlinear long-wave theory (shallow water theory), which accounts for advection and friction on the sea floor. However, a linear long-wave theory can also be applied in a marine area with a deeper water.

Most tsunamis occur when a crustal movement involves displacement of the sea floor area from several to a few dozen meters in the vertical direction, in a location where the sea floor area is less than several kilometers in depth, with a spatial spread of several dozens to several hundred kilometers in the horizontal direction. These tsunamis can be considered as waves with a sufficiently large scale in the horizontal direction rather than the vertical direction. On this basis, many aspects of the tsunami phenomenon can be described by theoretical formulae, applying long-wave theory.

Long wave theory is derived by treating the law of conservation of mass (continuity equation) and law of conservation of momentum (Euler's momentum equation) as base equations. For nonlinear long-wave theory (shallow water theory), which accounts for friction at the sea floor and a nonlinear effect by advection that cannot be ignored in a shallow marine area, the theoretical formula of an integral model, calculated by integrating from the sea floor to the water surface in the vertical direction, is expressed as follows:

$$\frac{\partial \eta}{\partial t} + \frac{\partial M}{\partial x} + \frac{\partial N}{\partial y} = 0 \quad (\text{Continuity equation})$$

$$\frac{\partial M}{\partial t} + \frac{\partial}{\partial x} \left[\frac{M^2}{D} \right] + \frac{\partial}{\partial y} \left[\frac{MN}{D} \right] + gD \frac{\partial \eta}{\partial x} + \frac{\tau_x}{\rho} = 0$$

(Euler's momentum equation)

$$\frac{\partial N}{\partial t} + \frac{\partial}{\partial x} \left[\frac{MN}{D} \right] + \frac{\partial}{\partial y} \left[\frac{N^2}{D} \right] + gD \frac{\partial \eta}{\partial y} + \frac{\tau_y}{\rho} = 0$$

In the momentum equation, the first term is the local acceleration term, the second and third terms are advection terms, fourth term is the pressure term, and the fifth term is the friction term. Friction term is generally expressed as the below, with a resistance term for a steady flow based on Manning formula.

$$\frac{\tau_x}{\rho} = \frac{gn^2}{D^{7/3}} M \sqrt{M^2 + N^2}, \quad \frac{\tau_y}{\rho} = \frac{gn^2}{D^{7/3}} N \sqrt{M^2 + N^2},$$

where, η (m) is the wave height, D (m) is the total water depth ($=h$ (m) + η (m)), g (m/s^2) is the gravitational acceleration, ρ (kg/m^3) is density, τ_x (N/m^2) and τ_y (N/m^2) are frictional forces at the sea floor in the x-axis and y-axis directions, respectively. M (m^2/s) and N (m^2/s) are linear flow rates in the x-axis and y-axis directions, respectively. $M = D\bar{u}$, and $N = D\bar{v}$, where \bar{u} and \bar{v} are average cross-sectional flow velocities in the x-axis and y-axis directions in the unit of m/s, respectively. n ($\text{m}^{-1/3} \cdot \text{s}$) is Manning's roughness coefficient.

The relationship between coordinates and each parameter is as shown in Figure 9.

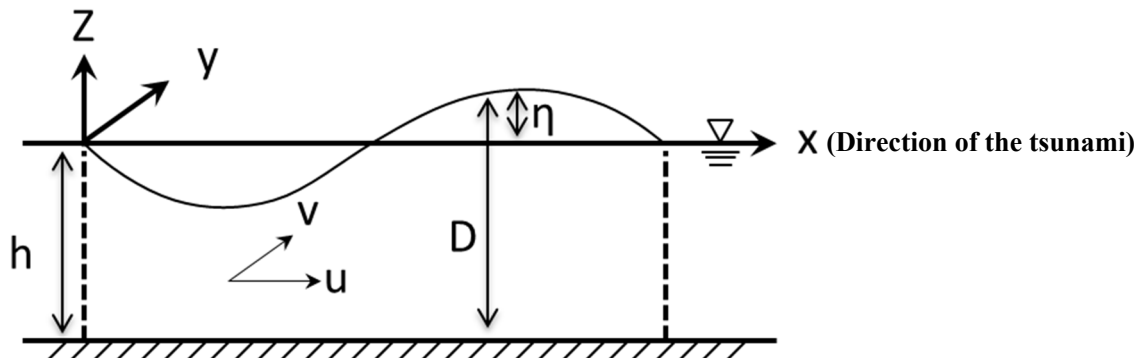


Figure 9. Coordinate system and parameters of the theoretical formula

In marine areas deeper than 50 m, the impact in the momentum equation of the advection and friction terms becomes smaller, and a linear long wave theory that omits these terms can be applied. Figure 10 covers the results of a numerical experiment in which each term in the momentum equation for shallow water theory was supplied by the one-dimensional propagation calculation (Imamura et al., 1986). In this case, it can be concluded that, if the only factors involved in momentum are local terms, and the pressure term is for water depth greater than 50 m, the size of the advection term at depths shallower than 50 m would be over 5% of the maximum value of the local term, and as much as 50% during a run-up.

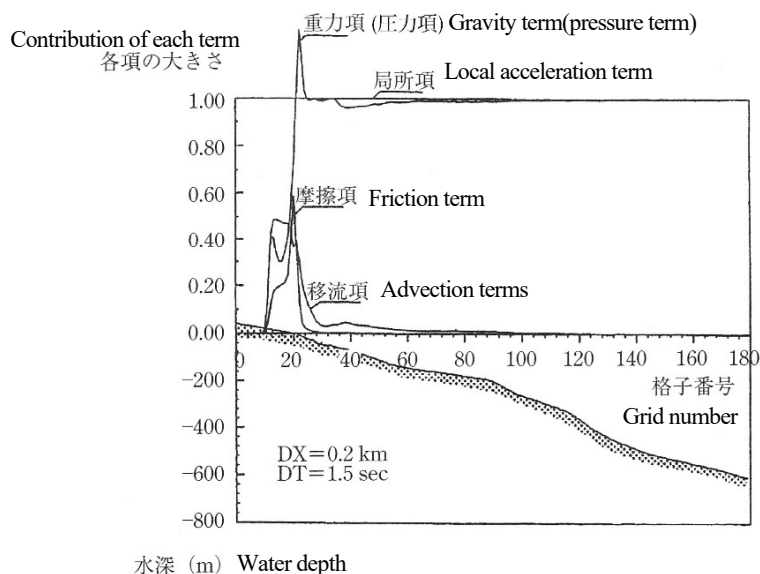


Figure 10. Comparison of the contribution of each term in the momentum equation using shallow water theory (Imamura et al., 1986). The maximum value of each term is normalized by the maximum value of a local term, while grid 20 on the horizontal axis is equivalent to the shoreline.

In a case where a detailed prediction is calculated for a tsunami that propagates for a long distance over a deep sea area, or for a tsunami that propagates over a broad shallow sea area in a near-tsunami, a dispersive wave theory needs to be utilized to account for dispersion of the tsunami (Iwase et al., 2002; Shigihara and Fujima, 2007).

(f) Boundary conditions

The sea (offshore) boundary is permeated by radiation with a perfect non-reflection, while the land boundary is typically considered as a run-up.

For a run-up calculation, the presence of water is determined for each computational grid per time step over the course of calculation, and flow needs to be configured by accounting for the relationship with the water level in adjacent computational grids. The methods by Iwasaki and Mano (1979) and Kotani et al. (1998) are frequently used for this calculation.

(g) Coefficient of roughness

Bottom friction in marine and terrestrial areas is taken into account by utilizing a coefficient of roughness.

The value of the Manning's roughness coefficient in a marine area is typically $n = 0.025 \text{ m}^{-1/3} \cdot \text{s}$. Various coefficients of roughness have been proposed for terrestrial areas, such as that estimated directly from the results of hydraulic model experiments (Fukuoka et al., 1994; Goto and Shuto, 1983), that which uses parameters such as the area occupancy ratio of a

house and house width (Aburaya and Imamura, 2002), that which provides an equivalent roughness in a uniform manner per area (Aida, 1977), and that which provides a roughness estimate for various types of land conditions (Kotani et al., 1998). All of these methods can be considered when configuring the coefficient of roughness for terrestrial areas in a detailed tsunami run-up calculation.

However, there are issues in applying the Manning formula on a run-up – particularly in the case of a rapidly varying, unsteady flow – and the resistance formula applicable to the tip of a tsunami running up is still a matter for research.

(h) Length of computation time and computational time step interval

The length of computational time for tsunami simulation needs to be configured so that the maximum tsunami height can be obtained while considering the topography of the tsunami, as well as that of the affected marine and terrestrial areas. The computational time step interval for tsunami simulations is configured appropriately by considering the stability of calculations.

The first wave is not necessarily the largest wave in a tsunami; the second wave often is. Therefore, a sufficient length of computational time should be configured to obtain the maximum height correctly.

Computational time interval should be configured by considering the stability, etc. of calculations against computational grid spacing, and should satisfy the following conditions (the Courant-Friedrichs-Lewy (CFL) Condition).

$$\Delta t \leq \frac{\Delta x}{\sqrt{2gh_{max}}}$$

In the CFL condition, Δt (s) is the computational time step interval, Δx (m) is the computational grid spacing, h_{max} (m) is the maximum water depth, and g (m/s^2) is the gravitational acceleration. Actual calculations will involve numerical errors and the nonlinearity of the phenomena, however, and the computational time interval should be configured sufficiently small compared to the CFL conditions.

2.2 Uncertainties in tsunami predictions

When configuring the characteristic source fault model, as well as uncertainties regarding the information that can be obtained in advance on the source fault, other uncertainties in tsunami predictions include an inability to obtain sufficient information on the following:

- Location and size of the assumed earthquake
- Spatial distribution of the slip amount in the source fault

Results for tsunami simulations obtained when configuring characterized earthquake fault models individually, involve the following uncertainties:

- Errors due to simplification of the source fault model, and expression using the finite number of parameters
- Errors from numerical calculations, including an error introduced by describing natural phenomena with a governing equation derived from certain approximations, an error introduced by discretizing the governing equations, and an error introduced by using an approximation of boundary conditions
- Errors contained in the topographic and bathymetric data

When sufficient information on the location and size of the assumed earthquake cannot be obtained, several characterized earthquake fault models should be configured using different locations and sizes, a tsunami prediction should be calculated for each model, and the tsunami should then be evaluated while accounting for uncertainties. When sufficient information on the spatial distribution of the slip in the source fault cannot be obtained, several characterized earthquake fault models should be configured, using different locations of the large and super large slip zones, as defined in 1.2 (a) and (c), then a tsunami simulation should be performed for each model, and the tsunami should be evaluated, while recognizing the uncertainties.

3. Validation of the characterized earthquake fault model

Damage records and observations for tsunamis are often available for the latest seismic activities, since interplate earthquakes considered in a tsunami evaluation have a short interval of occurrence, from several decades to over a hundred years. Therefore, the validity of the characterized earthquake fault model may be confirmed, and source fault characteristics may be revised by comparing such information with tsunami prediction results based on the methods discussed in this document. Items for comparison include estimated values based on tsunami trace height.

The validity of a characterized earthquake fault model can be confirmed by comparing the trace heights of tsunamis from previous earthquakes with the results from tsunami simulations obtained by applying a characterized earthquake fault model that corresponds to the earthquake. The model is considered to be valid if spatial features of the trace height can be explained to an acceptable level by simulations.

If spatial features of the trace height in some areas cannot be explained by tsunami simulations made using the characterized earthquake fault model, the model can be nonetheless considered valid in some circumstances. Such a situation could be if the model provided better explanation for spatial features of the trace height than tsunami prediction results based on several characterized earthquake fault models that used different configurations of the large and super large slip zone locations.

If sufficient information on the location and size of previous earthquakes cannot be obtained, the model can still be considered valid if a certain level of explanation can be provided for spatial features of the trace height. This may be achieved using a set of tsunami predictions based on several characterized earthquake fault models with differently configured locations and sizes.

When comparing trace height records with the results of tsunami simulations, caution should be observed, as a trace height may be disproportionately high, due to tsunami run-up being affected by the local topography. In addition, it should be recalled that some data may be affected by the tidal conditions applicable at the time of the trace height observations.

4. Appendix: Validation of the tsunami prediction method for earthquakes with characterized source faults (Tsunami Recipe)

This section compares the results of tsunami predictions for the 2011 off the Pacific coast of Tohoku earthquake (M 9.0) for which many observation records are available, using calculations based on available records, such as the tsunami trace height, and the "Tsunami prediction method for earthquakes with characterized source faults" (i.e., this "tsunami recipe"). The tsunami recipe will be validated by confirming the validity of the characterized earthquake fault model.

Parameters were configured based mainly on "The Long-term evaluation of subduction zone earthquakes along the area from off Sanriku to off Boso (ver. 2)" (Earthquake Research Committee, 2011) (i.e. "long-term evaluation").

The source fault model was configured to represent the region from the central Sanriku coast to the Ibaraki coast (including areas closer to the trench), as this region was identified as the source type of the off the Pacific coast of Tohoku earthquake in the long-term evaluation. Large slip zones and the super large slip zone were taken into account. The validation was performed with a model that configured the northern edge of the source fault as both the large slip zone and a super large slip zone, that being the configuration considered a model most suited for explaining the trace height left by the tsunami from the 2011 off the Pacific coast of Tohoku Earthquake.

Figure A1 and Tables A1 and A2 show an image of the characterized earthquake fault model and its parameters, respectively.

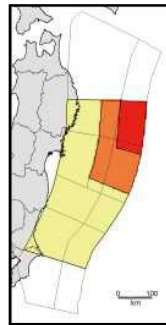


Figure A1. Characterized earthquake fault model: Red represents the super large slip zone, orange represents the large slip zone, and yellow represents the background zone

Table A1

Parameters for macroscopic source fault characteristics configured based on the tsunami recipe

Item	Value
Fault area S (km ²)	1.05×10^5
Seismic moment M_0 (Nm)	6.1×10^{22}
Moment magnitude M_w	9.1
Average stress drop $\Delta\sigma$ (MPa)	4.3
Modulus of rigidity μ (N/m ²)	5.0×10^{10}
Average slip D (m)	11.5

Table A2

Parameters for microscopic source fault characteristics configured based on the tsunami recipe

Item	Value
Average slip for the super large slip zone D_s (m)	46.0
Area of the super large slip zone S_s (km ²)	1.05×10^4
Average slip for the large slip zone D_L (m)	23.0
Area of the large slip zone S_L (km ²)	2.11×10^4
Average slip for the background zone D_B (m)	3.3
Area of the background zone S_B (km ²)	7.38×10^4

At this point, tsunami trace height predictions based on the tsunami recipe were relatively high compared to the actual trace heights left by the tsunamis. The reason for this is that the variable used was M_w 9.1, which was obtained by using an empirical relationship derived from the seismic moments and fault areas for earthquakes that have occurred on the Pacific side of Japan (Fujiwara et al., 2015), as shown in Table A1. Therefore, the average stress drop was adjusted to be M_w 9.0, to match the M 9.0 actually observed for the 2011 off the Pacific coast of Tohoku Earthquake, and the tsunami predictions were re-calculated, after re-configuring the parameters, as shown in Tables A3 and A4.

Table A3

Source fault characteristics parameter adjusted to be M_w 9.0

Item	Value
Fault area S (km ²)	1.05×10^5
Seismic moment M_0 (Nm)	4.2×10^{22}
Moment magnitude M_w	9.0
Average stress drop $\Delta\sigma$ (MPa)	3.0
Modulus of rigidity μ (N/m ²)	5.0×10^{10}
Average slip D (m)	8.0

Table A4

Macroscopic and microscopic source fault characteristics parameters adjusted to be M_w 9.0

Item	Value
Average slip for the super large slip zone D_s (m)	32.0
Area of the super large slip zone S_s (km ²)	1.05×10^4
Average slip for the large slip zone D_L (m)	16.0
Area of the large slip zone S_L (km ²)	2.11×10^4
Average slip for the background zone D_B (m)	2.3
Area of the background zone S_B (km ²)	7.38×10^4

Trace heights left by tsunamis were based on the data of The 2011 Tohoku Earthquake Tsunami Joint Survey (TTJS) Group (<http://www.coastal.jp/tjt/>, Oct. 3, 2012) and those that matched the following conditions were extracted (Korenaga et al., 2013).

- Trace reliability grade A, as defined by The 2011 Tohoku Earthquake Tsunami Joint Survey (TTJS) Group.
- Trace height at or over 50 cm, and coastal upstream distance known within 100 m

- If there are structures nearby that cannot be expressed on a 50 m computational grid, the computational grid of the coast and trace point found were found to be within 50 m of each other

Comparisons of trace heights extracted from Aomori Prefecture to Chiba Prefecture (●), and calculated heights for the computational grid for the coastal areas closest to the trace height locations (◆) are shown in Figure A2. The height calculated by the M_w 9.0 model was able to match the trace heights, in general, and the validity of the characterized earthquake fault model can be confirmed by this result.

However, the trace height was not matched very well by the calculated height in some areas, particularly in Fukushima Prefecture, for example, which highlights the limit of the characterized earthquake fault model. This point needs to be kept in mind when using the characterized earthquake fault model

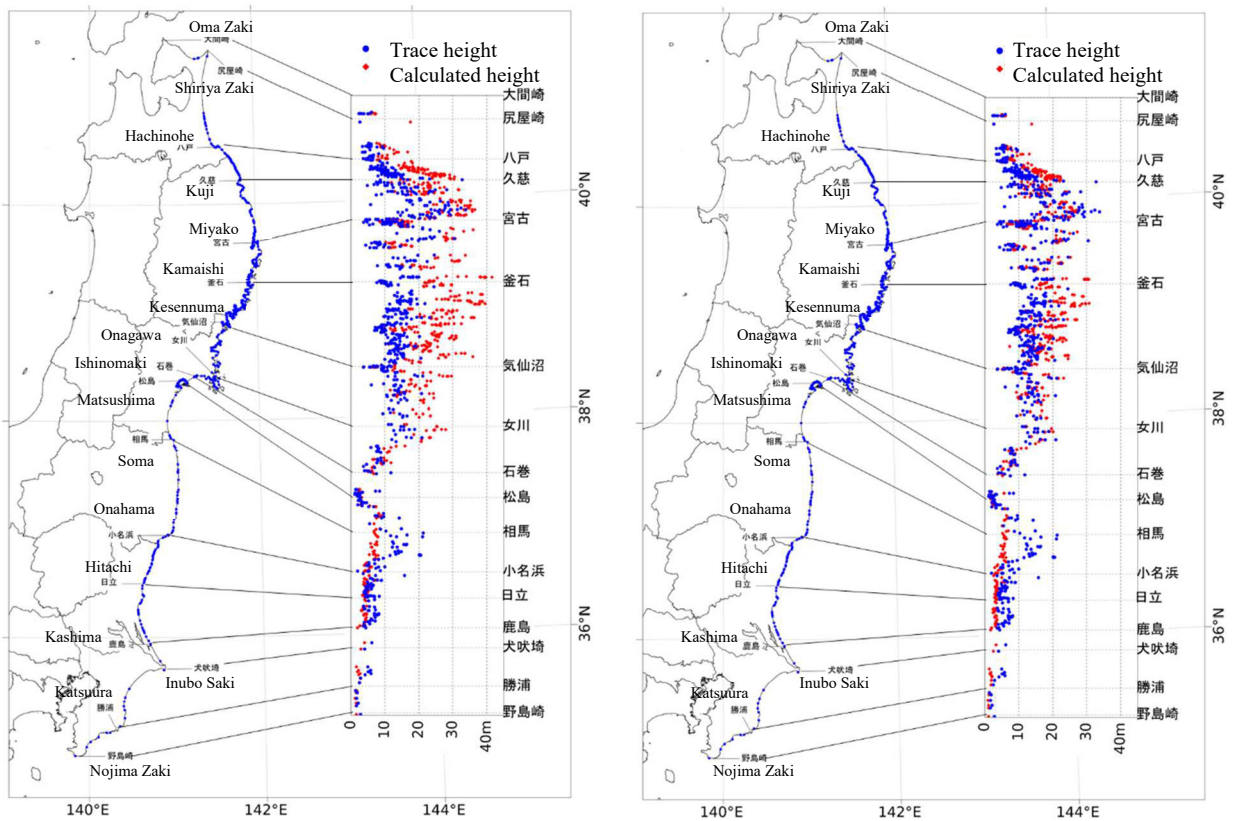


Figure A2. Comparison of actual trace heights and calculated heights obtained by using the characterized earthquake fault model; the calculated heights in the left figure were obtained using the M_w 9.1 model, while those for the right figure were obtained using the M_w 9.0 model.

5. References

- Aburaya T. and F. Imamura (2002): A Proposal of tsunami inundation simulation using a synthesized equivalent roughness model, *Proceed. Coast. Eng., JSCE*, **49**, 276-280 (in Japanese).
- Aida, I. (1977): Numerical Experiments for Inundation of Tsunamis. : Susaki and Usa, in Kochi Prefecture, *Bull. Earthq. Res. Inst., Univ. Tokyo*, **52**, 441-460 (in Japanese).
- Ben-Menahem, A., and M. Rosenman (1972): Amplitude Patterns of Tsunami Waves from Submarine Earthquakes, *J. Geophys. Res.*, **77**, 3097-3128, doi:10.1029/JB077i017p03097.
- Bilek, S. L., and T. Lay (1999): Rigidity variations with depth along interplate megathrust faults in subduction zones, *Nature*, **400**, 443-446, doi:10.1038/22739.
- Cabinet Office (2012) : The Committee for Modeling a Nankai Trough Megaquake (second report) : Tsunami models – on the fault models for tsunami simulation and their expected heights and inundation areas, http://www.bousai.go.jp/jishin/nankai/model/pdf/20120829_2nd_report01.pdf (in Japanese).
- Earthquake Research Committee, The Headquarter for the Earthquake Research Promotion (2011): The Long-term evaluation of subduction zone earthquakes along the area from off Sanriku to off Boso (ver. 2), https://www.jishin.go.jp/main/chousa/kaikou_pdf/sanriku_boso_4.pdf (in Japanese).
- Earthquake Research Committee, The Headquarter for the Earthquake Research Promotion (2012): Japan Integrated Velocity Structure Model (provisional version), Appendix 2, the Long-period ground motion hazard map, https://www.jishin.go.jp/main/chousa/12_choshuki/choshuki2012_a2.pdf (in Japanese).
- Earthquake Research Committee, The Headquarter for the Earthquake Research Promotion (2016): Strong ground motion prediction method for earthquakes with specified source faults ("Recipe") ver. 2016, https://www.jishin.go.jp/main/chousa/16_yosokuchizu/recipe.pdf (in Japanese).
- Eshelby, J. D. (1957): The determination of the elastic field of an ellipsoidal inclusion, and related problems, *Proceedings of the Royal Society*, **A241**, 376-396.
- Fujii, Y. and K. Satake (2007): Tsunami Source of the 2004 Sumatra–Andaman Earthquake Inferred from Tide Gauge and Satellite Data, *Bull. Seis. Soc. Am.*, **97**, S192-S207, doi:10.1785/0120050613.
- Fujii, Y. and K. Satake (2013): Slip Distribution and Seismic Moment of the 2010 and 1960 Chilean Earthquakes Inferred from Tsunami Waveforms and Coastal Geodetic Data, *Pure Appl. Geophys.*, **170**, 1493-1509, doi:10.1007/s00024-012-0524-2.
- Fujiwara, H., K. Hirata, H. Nakamura, M. Osada, N. Morikawa, S. Kawai, T. Ohsumi, S. Aoi, H. Matsuyama, N. Toyama, T. Kito, Y. Murasima, Y. Murata, T. Inoue, R. Saito, S. Akiyama, M. Korenaga, Y. Abe, and N. Hashimoto (2015): An Approach to Tsunami Hazard Assessment along the Northeastern Coastal Area in Japan-Method and Preliminary Results-, *Tech. Note National Res. Inst. Earth Sc. Disaster Prevention*, **400** (in Japanese).
- Fukao, Y. (1979): Tsunami Earthquakes and Subduction Processes Near Deep-Sea Trenches, *J. Geophys. Res.*, **84**, 2303-2314, doi:10.1029/JB084iB05p02303.
- Fukuoka, S., M. Kawashima, N. Matsunaga, and H. Maeuchi (1994): Flooding water over a crowded urban district, *Doboku Gakkai Ronbunshu*, 491/II-27, 51-60 (in Japanese).
- Goto, C., and N. Shuto (1983): Effects of large obstacles on tsunami inundations, *Tsunamis: Their Science and Engineering*, Terra Scientific Publishing Company, 511-525.
- Gusman, A. R., Y. Tanioka, S. Sakai and H. Tsushima (2012): Source model of the great 2011 Tohoku earthquake estimated from tsunami waveforms and crustal deformation data, *Earth Planet. Sci. Lett.*, **341-344**, 234-242.

- Gusman, A. R., S. Murotani, K. Satake, M. Heidarzadeh, E. Gunawan, S. Watada, and B. Schurr (2015): Fault slip distribution of the 2014 Iquique, Chile, earthquake estimated from ocean-wide tsunami waveforms and GPS data, *Geophys. Res. Lett.*, **42**, 1053-1060, doi: 10.1002/2014GL062604.
- Hasegawa, K., T. Suzuki, K. Inagaki, and N. Shuto (1987): A study on the mesh size and time increment in the numerical simulation of tsunamis, *Doboku Gakkai Ronbunshu*, **381/II-7**, 111-120 (in Japanese).
- Hashimoto, C., A. Noda, T. Sagiya and M. Matsu'ura (2009): Interplate seismogenic zones along the Kuril–Japan trench inferred from GPS data inversion, *Nature Geoscience*, **2**, 141-144, doi:10.1038/ngeo421.
- Imamura, F., C. Goto, and N. Shuto (1986): Research on the possibility of the numerical prediction of tsunami - Accuracy of tsunami numerical simulation-, *Bull. Tsunami Eng. Lab., Faculty of Eng., Tohoku Univ.*, **3**, 23-88 (in Japanese).
- Irikura, K., and H. Miyake (2001): Prediction of Strong Ground Motions for Scenario Earthquakes, *J. Geogra.*, **110**, 849-875 (in Japanese).
- Iwasaki, T., and A. Mano (1979): Numerical simulation of two-dimensional tsunami run-up on the Euler coordinates, *Proceed. Coast. Eng., JSCE*, **26**, 70-74 (in Japanese).
- Iwase, H., T. Mikami, C. Goto, K. Fujima (2002): A comparative study of nonlinear dispersive long wave equations for numerical simulation of tsunami, *Doboku Gakkai Ronbunshu*, **705/II-59**, 129-138 (in Japanese).
- Iwata, T. and K. Asano (2011): Characterization of the Heterogeneous Source Model of Intraslab Earthquakes Toward Strong Ground Motion Prediction, *Pure Appl. Geophys.*, **168**, 117-124, doi:10.1007/s00024-010-0128-7.
- Johnson, J. M., K. Satake, S. R. Holdahl and J. Sauber (1996): The 1964 Prince William Sound earthquake: Joint inversion of tsunami and geodetic data, *J. of Geophys. Res.*, **101**, 523-532, doi:10.1029/95JB02806.
- Johnson, J. M. and K. Satake (1999): Asperity Distribution of the 1952 Great Kamchatka Earthquake and its Relation to Future Earthquake Potential in Kamchatka, *Pure Appl. Geophys.*, **154**, 541-553, doi:10.1007/s000240050243.
- Kajiura, K. (1963): The Leading Wave of a Tsunami, *Bull. Earthq. Res. Inst.*, **41**, 535-571.
- Kajiura, K. (1970): Tsunami Source, Energy and the Directivity of Wave Radiation, *Bull. Earthq. Res. Inst.*, **48**, 835-869.
- Kanamori, H. and D. L. Anderson (1975): Theoretical basis of some empirical relations in seismology, *Bull. Seis. Soc. Am.*, **65**, 1073-1095.
- Kawata, Y., Y. Okumura, and S. Koshimura (2006): Effect of dynamic characteristics of fault rupture on the occurrence of tsunami, *Proceed. Coast. Eng., JSCE*, **53**, 291-295 (in Japanese).
- Korenaga, M., Y. Abe, N. Hashimoto, S. Akiyama, and H. Fujiwara (2013): The uncertainties in the probabilistic tsunami hazard evaluation, *Proceed. JpGU2013, SSS35-P06* (in Japanese).
- Kotani, M., F. Imamura, and N. Shuto (1998): Tsunami run-up calculation and damage estimation method with GIS, *Proceed. Coast. Eng., JSCE*, **45**, 356-360 (in Japanese).
- Lorito, S., F. Romano, S. Atzori, X. Tong, A. Avallone, J. McCloskey, M. Cocco, E. Boschi and A. Piatanesi (2011): Limited overlap between the seismic gap and coseismic slip of the great 2010 Chile earthquake, *Nature Geoscience*, **4**, 173–177, doi:10.1038/ngeo1073.
- Mansinha, L. and D. E. Smylie (1971): The displacement fields of inclined faults, *Bull. Seis. Soc. Am.*, **61**, 1433-1440.
- Meade, B. J. (2007): Algorithms for the calculation of exact displacements, strains, and stresses for triangular dislocation elements in a uniform elastic half space, *Computers & geosciences*, **33**, 1064-1075, doi:10.1016/j.cageo.2006.12.003.

- Ministry of Land, Infrastructure, Transport and Tourism (Water and Disaster Management Bureau, and National Institute for Land and Infrastructure Management) (2012): Guidance for setting tsunami inundation assumptions (Ver.2.00), https://www.mlit.go.jp/river/shishin_guideline/bousai/saigai/tsunami/shinsui_settei.pdf (in Japanese).
- Murashima, Y., F. Imamura, H. Takeuchi, T. Suzuki, K. Yoshida, M. Yamazaki, K. Matsuda (2006): Adaptability of Aircraft-mounted Laser Data for Tsunami Inundation Prediction, *Proceed. Coast. Eng., JSCE*, **53**, 1336-1340 (in Japanese).
- Murotani, S., H. Miyake and K. Koketsu (2008): Scaling of characterized slip models for plate-boundary earthquakes, *Earth Planets Space*, **60**, 987–991.
- Murotani, S., K. Satake and Y. Fujii (2013): Scaling relations of seismic moment, rupture area, average slip, and asperity size for M~9 subduction-zone earthquakes, *Geophys. Res. Lett.*, **40**, 5070–5074, doi:10.1002/grl.50976.
- Nishimura, T. (2012): Crustal deformation of northeastern Japan based on geodetic data for recent 120 years, *J. Geol. Soc. Japan*, **118**, 278-293, doi:10.5575/geosoc.2012.0027 (in Japanese).
- Okada, Y. (1985): Surface deformation due to shear and tensile faults in a half-space, *Bull. Seis. Soc. Am.*, **75**, 1135-1154.
- Okada, Y. (1992): Internal deformation due to shear and tensile faults in a half-space, *Bull. Seis. Soc. Am.*, **82**, 1018-1040.
- Romano, F., A. Piatanesi, S. Lorito, N. D'Agostino, K. Hirata, S. Atzori, Y. Yamazaki and M. Cocco (2012): Clues from joint inversion of tsunami and geodetic data of the 2011 Tohoku-oki earthquake, *Scientific reports*, **2**, 385, doi:10.1038/srep00385.
- Satake, K., K. Hirata, S. Yamaki and Y. Tanioka (2006): Re-estimation of tsunami source of the 1952 Tokachi-oki earthquake, *Earth Planets Space*, **58**, 535-542.
- Satake, K., Y. Fujii, T. Harada and Y. Namegaya (2013): Time and Space Distribution of Coseismic Slip of the 2011 Tohoku Earthquake as Inferred from Tsunami Waveform Data, *Bull. Seis. Soc. Am.*, **103**, 1473-1492, doi:10.1785/0120120122.
- Sato, R. (1971): Crustal Deformation due to Dislocation in a Multi-layered Medium, *J. Phys. Earth*, **19**, 31-46.
- Sato, R. and M. Matsu'ura (1973): Static deformations due to the fault spreading over several layers in a multi-layered medium, *J. Phys. Earth*, **21**, 227-249.
- Sato, R. (1989): Handbook of earthquake fault parameters in Japan, Kajima Publisher (in Japanese).
- Shigihara, Y., K. Fujima (2007): Adequate numerical scheme for dispersive wave theory for tsunami simulation and development of new numerical algorithm, *Doboku Gakkai Ronbunshu B*, **63**, 51-66 (in Japanese).
- Song, T. R. A., and M. Simons (2003): Large Trench-Parallel Gravity Variations Predict Seismogenic Behavior in Subduction Zones, *Science*, **301**, 630-633.
- Sugino, H., C. Wu, M. Korenaga, M. Nemoto, Y. Iwabuchi and K. Ebisawa (2013): Analysis and Verification of the 2011 Tohoku Earthquake Tsunami at Nuclear Power Plant Sites, *J. Jap. Assoc. Earthq. Eng.*, **13**, 2_2-2_21 (in Japanese).
- Sugino, H., Y. Iwabuchi, N. Hashimoto, K. Matsusue, K. Ebisawa, H. Kameda, and F. Imamura (2014): The Characterizing Model for Tsunami Source regarding the Inter-plate Earthquake Tsunami, *J. Jap. Assoc. Earthq. Eng.*, **14**, 5_1-5_18 (in Japanese).
- Sugiyama, Y. (2004): Asperities and multi-segment ruptures in subduction zones and inland active fault systems, *Proceedings of International Conference in Commemoration of 5th Anniversary of The 1999 Chi-Chi Earthquake, Taiwan*, 1-9.
- Suppasri, A., S. Koshimura, and F. Imamura (2011): Developing tsunami fragility curves based on the satellite remote sensing and the numerical modeling of the 2004 Indian Ocean tsunami in Thailand, *Natural Hazards and Earth System Science*, **11**, 173-189, doi:10.5194/nhess-11-173-2011.

- Tajima, R., Y. Matsumoto, H. Si, and K. Irikura (2013): Comparative Study on Scaling Relations of Source Parameters for Great Earthquakes in Inland Crusts and on Subducting Plate-Boundaries, *Zisin ser. II*, **66**, 31-45, doi:10.4294/zisin.66.31 (in Japanese).
- Tanioka, Y., and K. Satake (1996): Tsunami generation by horizontal displacement of ocean bottom, *Geophys. Res. Lett.*, **23**, 861-864.
- Tanioka, Y. and K. Satake (2001a): Detailed coseismic slip distribution of the 1944 Tonankai earthquake estimated from tsunami waveforms, *Geophys. Res. Lett.*, **28**, 1075-1078.
- Tanioka, Y., and K. Satake (2001b): Coseismic slip distribution of the 1946 Nankai earthquake and aseismic slips caused by the earthquake, *Earth Planets Space*, **53**, 235-241, doi:10.1186/BF03352380.
- Tanioka, Y., K. Hirata, R. Hino, and T. Kanazawa (2004): Detailed Slip Distribution of the 2003 Tokachi-oki Earthquake Estimated from Tsunami Waveforms, *Zisin ser. II*, **57**, 75-81 (in Japanese).
- Thomas, A. L. (1993): Poly3D: A three-dimensional, polygonal element, displacement discontinuity boundary element computer program with applications to fractures, faults, and cavities in the Earth's crust, Doctoral dissertation, Stanford University.
- The Tsunami Evaluation Subcommittee, The Nuclear Civil Engineering Committee, JSCE (Japan Society of Civil Engineers) (2016) : Tsunami Assessment Method for Nuclear Power Plants in Japan (in Japanese).
- Tsushima, H., R. Hino, Y. Tanioka, F. Imamura and H. Fujimoto (2012): Tsunami waveform inversion incorporating permanent seafloor deformation and its application to tsunami forecasting, *J. Geophys. Res.*, **117**, B03311, doi:10.1029/2011JB008877.
- Wells, R. E., R. J. Blakely, Y. Sugiyama, D. W. Scholl and P. A. Dinterman (2003): Basin-Centered asperities in great subduction zone earthquakes: A link between slip, subsidence, and subduction erosion?, *J. Geophys. Res.*, **108**, 2507, doi:10.1029/2002JB002072.
- Yamanaka, Y. and K. Shimazaki (1990): Scaling Relationship between the Number of Aftershocks and the Size of the Main Shock, *J. Phys. Earth*, **38**, 305-324.
- Yamashita, T. and R. Sato (1974): Generation of tsunami by a fault model, *J. Phys. Earth*, **22**, 415-440.

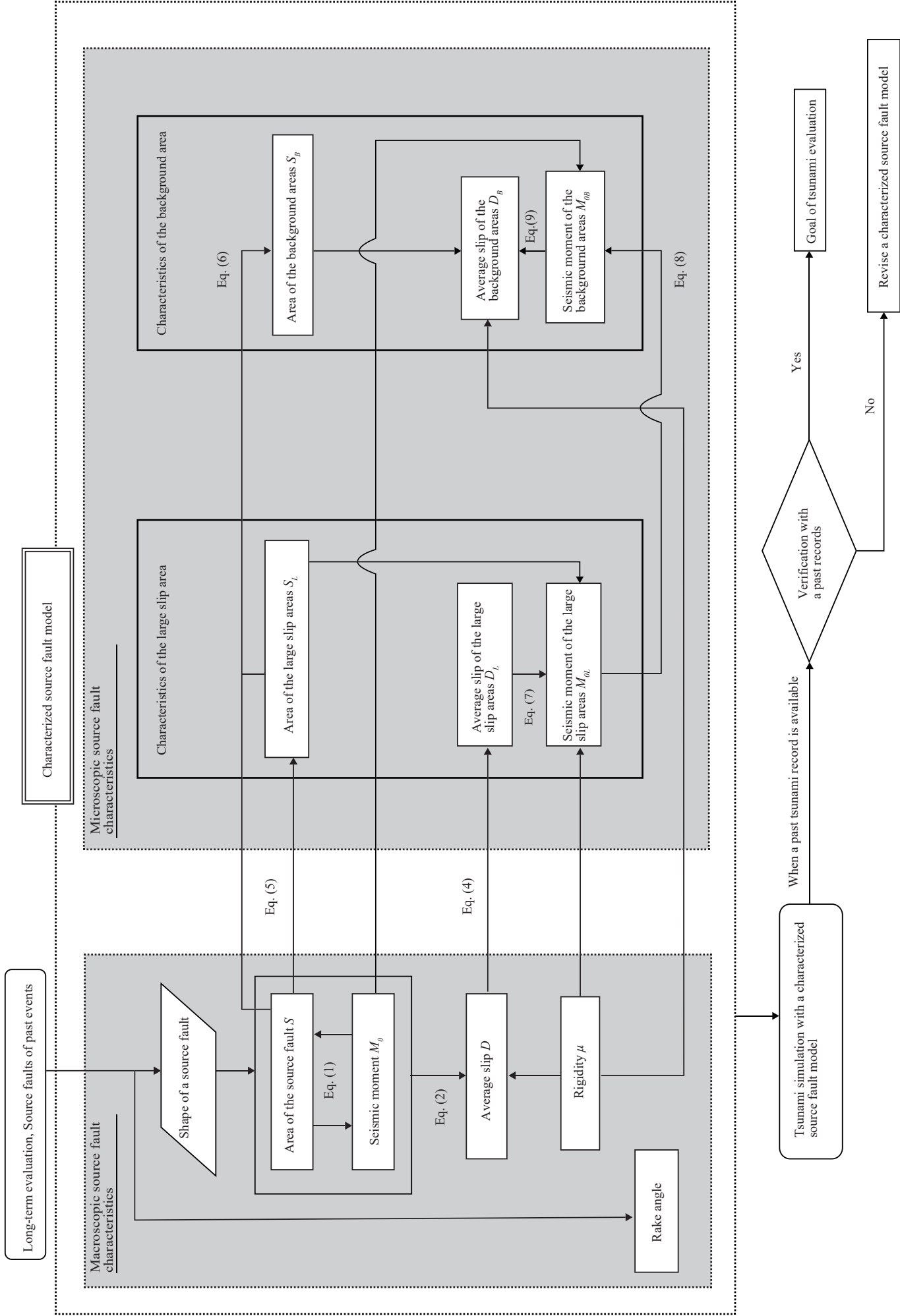


Figure F1. Flowchart used for configuration of source fault characteristic parameters for interplate earthquakes (large slip zones) configured

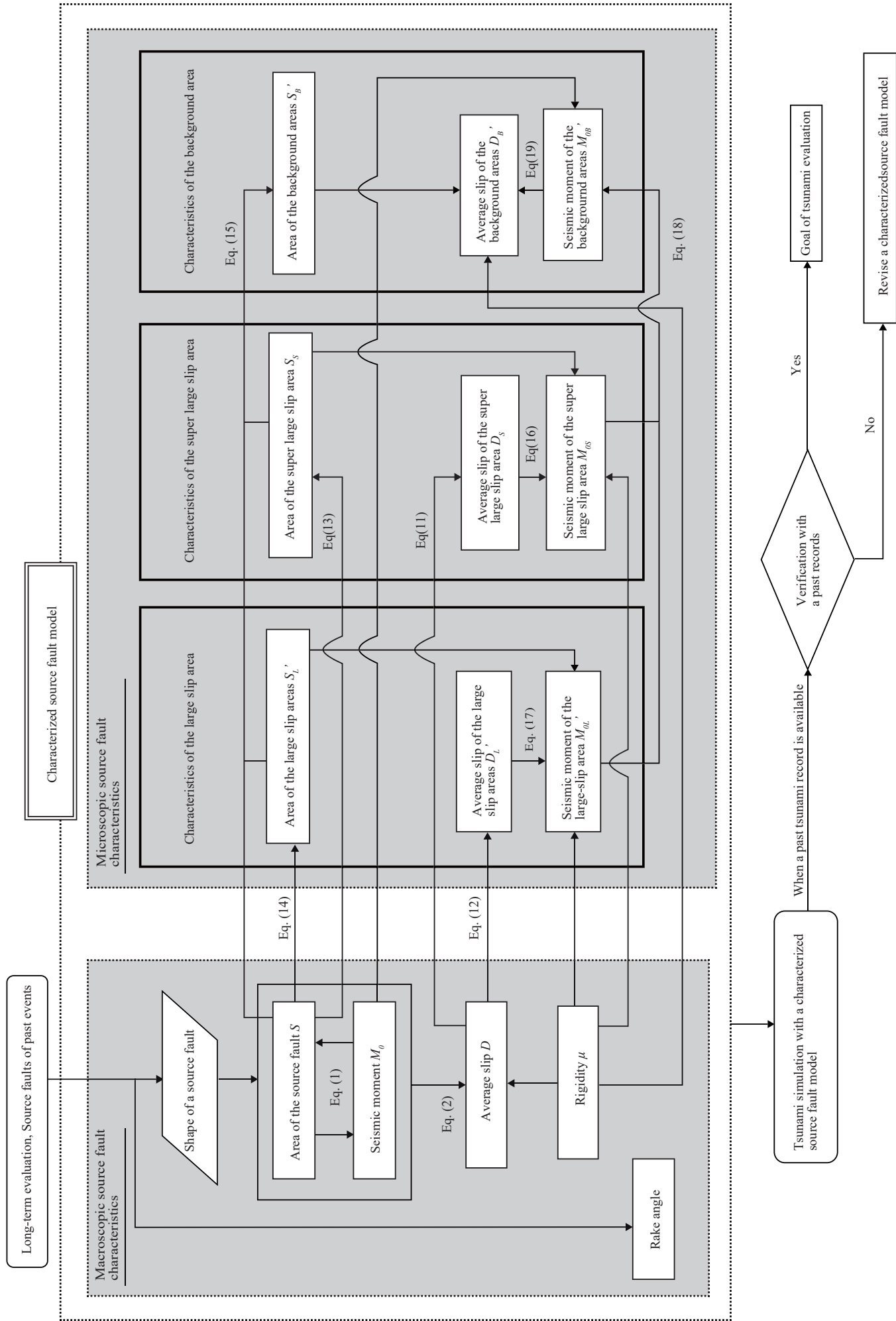


Figure F2. Flowchart used for configuration of source fault characteristics for interplate earthquakes (large slip zones and super large slip zones configured)